Author(s): Luoma, M.; García, F.; Äystö, J.; Blatz, T.; Chokheli, D.; Flemming, H.; Götzen, K.; Grahn, T.; Jokinen, A.; Karagiannis, C.; Kurz, N.; Löchner, S.; Nociforo, C.; Rinta-Antila, S.; Schmidt, C. J.; Simon, H.; Turpeinen, R.; Voss, B.; Wieczorek, P.; Winkler, M.

Title: In-beam test results of the Super-FRS GEM-TPC detector prototype with relativistic uranium ion beam

Year: 2023

Version: Published version

Nuclear Inst. and Methods in Physics Research, A 1052 (2023) 168262

Contents lists available at ScienceDirect

Nuclear Inst. and Methods in Physics Research, A

journal homepage: www.elsevier.com/locate/nima

Full Length Article

In-beam test results of the Super-FRS GEM-TPC detector prototype with relativistic uranium ion beam

M. Luoma [a,b,*], F. García [a], J. Äystö [a,b], T. Blatz [c], D. Chokheli [d], H. Flemming [c], K. Götzen [c], T. Grahn [a,b], A. Jokinen [a,b], C. Karagiannis [c], N. Kurz [c], S. Löchner [c], C. Nociforo [c], S. Rinta-Antila [a,b], C.J. Schmidt [c], H. Simon [c], R. Turpeinen [a], B. Voss [c], P. Wieczorek [c], M. Winkler [c]

[a] Helsinki Institute of Physics, P.O. Box 64, FI-00014, University of Helsinki, Finland
[b] University of Jyvaskyla, Department Of Physics, P.O Box 35, FI-40014, University of Jyvaskyla, Finland
[c] GSI Helmholzzentrum für Schwerionenforschung GmbH, Darmstadt 64291, Germany
[d] Georgian Technical University, Tbilisi, Georgia

ARTICLE INFO

Keywords:
GEM-TPC
Tracking
Clusterization
Super-FRS
FAIR

ABSTRACT

As an essential part of the Super-FRS particle identification, the GEM-TPC detector in a twin field-cage configuration will provide position information at up to 1 MHz counting rate with a spatial resolution < 1 mm and with tracking efficiency > 95 %. This detector is designed to provide particle-beam tracking information of projectiles ranging from protons to uranium. The performance of the GEM-TPC detector in a single field-cage configuration and newly integrated AWAGS readout electronics with a differential output was studied at the FRS for the response to the uranium beam at 850 MeV/u with intensity up to 1000 ions/spill. The result shows that a clusterization algorithm developed for this analysis works properly. The spatial resolution of 0.74–0.81 mm, a detection efficiency > 99 %, and a tracking efficiency > 96 % were found. This work describes the methodology used to achieve such results in detail.

1. Introduction

The Facility for Antiproton and Ion Research in Europe GmbH (FAIR) [1] in Darmstadt, Germany, will be one of the largest accelerator laboratories worldwide. One of the main parts of FAIR will be the Superconducting FRagment Separator (Super-FRS) [2]. The Super-FRS intends to be an extremely powerful in-flight magnetic separator that can produce, separate, and deliver high-energy radioactive beams.

The Super-FRS can be used as an independent experimental device and as a high-resolution spectrometer [3]. It is designed to deliver a high energy and spatially separated beams of exotic nuclei of all elements up to uranium. Compared to the existing FRagment Separator (FRS) [4], major improvements will be applied to the Super-FRS such as higher primary beam intensities. In addition, momentum and angular acceptance of Super-FRS will be more than twice larger. The resulting increased beam intensities in the Super-FRS require some upgrades for the standard particle detectors used in the FRS, such as higher counting rate capabilities.

The Super-FRS is divided into two parts, the pre-separator and the main-separator with three exits to the experimental stations, the low-energy branch, the high-energy branch, and the ring branch. Along the Super-FRS beam line, there will be different in-beam detector systems for the diagnostics and tuning, depending on their location. The diagnostic setup at the final focal plane of the main-separator will consist mainly of transmission particle detectors to measure energy-loss, time-of-flight, and position of the particle beam, all of them working on an event-by-event basis.

At the FRS and in the future Super-FRS, the particles are identified by magnetic rigidity ($B\rho$) analysis, time-of-flight (TOF) determination, and energy loss (ΔE) measurement, i.e. by the so-called $B\rho$-TOF-ΔE method [2,4]. Currently, the tracking in FRS is done by conventional Time Projection Chambers (TPC), with a tracking efficiency of 98% at 50 kHz [5]. However, one of the design goals for the Super-FRS is to operate at counting rates of about 1 MHz, maintaining a position resolution of < 1 mm and keeping the perturbance to the traversing beam minimal, thus requiring a minimal amount of homogeneous material along the beam path. Moreover, depending on the conditions of the experiment, some of the tracking detectors need to be able to operate not only in a vacuum but also in the air.

The particle identification in the Super-FRS will be performed partly by a set of Time Projection Chambers with Gas Electron Multipliers

* Corresponding author at: Helsinki Institute of Physics, P.O. Box 64, FI-00014, University of Helsinki, Finland.
E-mail address: minna.a.m.luoma@jyu.fi (M. Luoma).

https://doi.org/10.1016/j.nima.2023.168262
Received 15 October 2022; Received in revised form 14 March 2023; Accepted 1 April 2023
Available online 3 April 2023

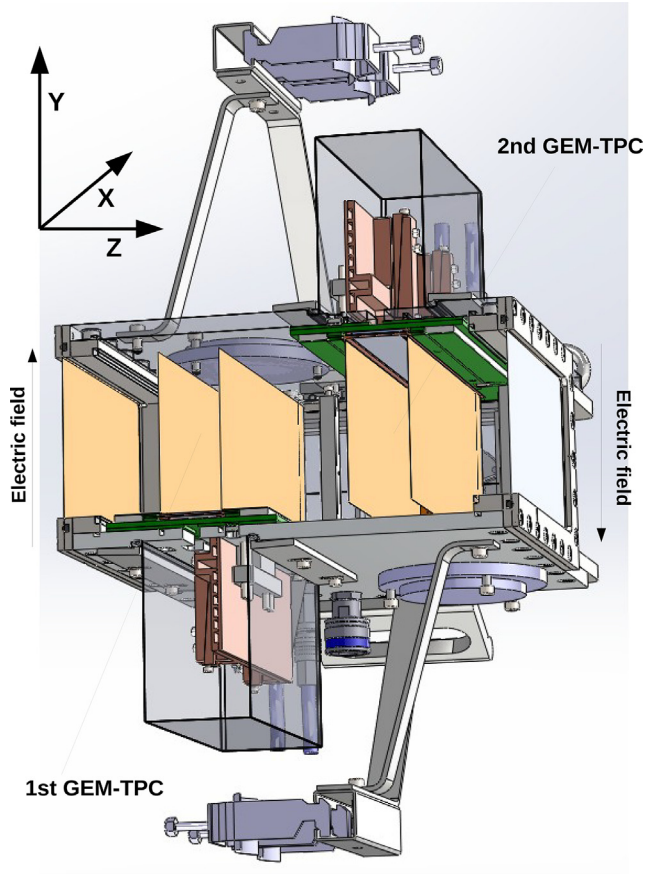

Fig. 1. The layout of the twin GEM-TPC detector where electric fields are in opposite directions together with the used coordinate system. See more technical details in the Ref. [10] and dimensions in Fig. 2(b).

(GEM-TPC) in twin field-cage configuration [6]. The GEM-TPC in a twin configuration has two GEM-TPCs inside a single vessel containing the same gas volume (see Fig. 1). One of the GEM-TPCs is flipped in the middle plane with respect to the second one in such a way that the electric fields inside both field-cages are in opposite directions. The GEM-TPC provides the position information [7] and the identification of the isotopes is complemented by the Time-of-Flight detectors [8] and the Multi-Sample Ionization Chambers (MUSIC) [9].

The GEM-TPC prototype HGB4 has been tested earlier with a uranium primary beam [11]. The main object of the investigation in the present in-beam test has been the response of the detector with new integrated readout electronics. Therefore, one of the goals of the current work is to study the performance of the GEM-TPC detector, with the integrated Low Noise Amplifier With Adaptive Gain Settings (AWAGS) ASIC [12,13] with a differential output. This was the first in-beam test where the AWAGS was used with the GEM-TPC. The collected data allowed the development and characterization of a clusterization algorithm for the data analysis. This can be further used to determine the position of the projectiles in space, thus deriving the coordinates of interactions and their arrival times. This gave an opportunity to extract the spatial resolution as well as tracking and detection efficiencies.

The following chapters describe the experimental setup, the GEM-TPC, and the developed data analysis method. Special attention will be given to the calibrations and alignment of the conventional TPCs as reference trackers coupled with the Device Under Test (DUT), a GEM-TPC in a single field-cage configuration.

2. Experimental setup

The experimental setup is composed by two TPCs (TPC41 and TPC42) placed on the beamline for tracking purposes, followed by a plastic scintillator (SC41) for providing the trigger signal, thus setting the starting time of each event, hereafter t_0. The DUT, a GEM-TPC, is placed on the beamline downstream (see Fig. 2(a) and the dimensions of the detectors Fig. 2(b)). The DUT assembled at the focal plane of FRS (S4) is shown in Fig. 3.

The gas mixture in use was P10 (90% Ar, 10% CH4) at atmospheric pressure and room temperature. The electric field strength inside the field-cage was varied from 90 V/cm to 320 V/cm. The primary beam of ^{238}U at 850 MeV/u with a spill length between 2 s to 8 s and intensities of 100–1000 ions/spill were delivered by the FRS.

The coordinate system in the present in-beam test is shown in Fig. 1, the z-axis is set parallel to the beam direction and orthogonal to the DUT planes, the x-axis is in the horizontal, and the y-axis is in the vertical direction. The x coordinate is given by the location of the strips, and the y coordinate by the reconstructed drift time in the DUT.

The GEM-TPC consists of a field-cage (see Fig. 4), similar to the TPC [5], a stack made of Gas Electron Multiplier (GEM) foils [14] used for the initial electron ionization amplification, which for this particular case is a set of three GEM foils and the front-end electronics.

The field-cage has a set of 32 strips with a pitch of 3.12 mm covering 100 mm of drift length [15]. The strips on the field-cage are on both sides of 10 μm thick aluminized mylar foil, which forms its walls.

The electrical connection is made by a resistor divider, where the first strip on top is connected to the cathode, and the last strip, on the bottom is connected to the top electrode of the first GEM foil [15]. In such a way, an electric field strength can be applied to the whole volume of the field-cage.

The GEM-TPC bias is done by two high-voltage channels. One is connected to the cathode, which has a high potential, but low current to provide the voltages to all strips of the field-cage, and the second one with a lower potential but with a higher current is used to power the GEM stack.

The readout plane of the DUT consists of 512 parallel strips with a pitch of 0.4 mm (strip width 0.25 mm) parallel to the beam direction. However, only half of them were read out due to the limited number of readout channels available. During the run, a group of 32 channels were found faulty, resulting in 224 channels that were used in the analysis.

The signals induced on each strip were used to determine the coordinates of an event. These signals were picked up either from the bottom of the third GEM foil or the strips of the readout strip plane (see Fig. 5).

The AWAGS readout electronics read the charge from the strips and generated analog signals which were fed into the FEBEX3b digitizer (Front End Board with optical link EXtension) [16], shown in Fig. 6. In the present in-beam test, strips were read out by a set of 14 FEBEX3b digitizers. The FEBEX3b is a 14-bit ADC used to digitize waveforms of both polarities. In the case of the DUT, the polarity of the signals is always negative, and the effective dynamic range is half as a consequence, thus allowing $2^{13} = 8192$ ADC counts. One FEBEX3b board has 16 channels sampling at 50 MHz rate, hence with a 20 ns sampling time [17]. This last will be later the granularity on the discretization of each signal.

The Multi Branch System (MBS) [18], which allows the data collection and synchronization within a single event, was used as the Data Acquisition System (DAQ). Therefore, all the detectors are synchronized by the same timestamp value. The output of the digitizers is transferred to the PCI-Express Optical Receiver (PEXOR) [19], which connects front-end cards to the DAQ computer. The PC-based Trigger Module (TRIXOR) [20] is controlled by the PEXOR, and it is used for the data synchronization, starting and stopping the data taking.

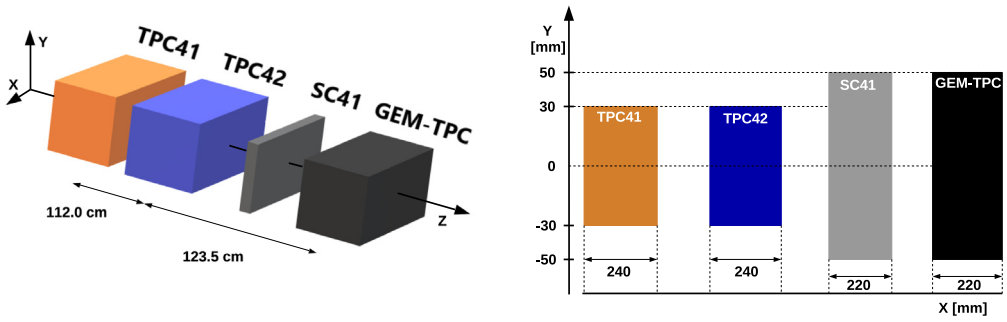

(a) (b)

Fig. 2. (a) A schematic view of the experimental setup located on the final focal plane of FRS is shown. The TPC41, TPC42, SC41, and the GEM-TPC were all aligned in the middle of the horizontal and vertical planes. (b) A side view of the setup is shown, highlighting the dimensions of the detector active areas in the horizontal and vertical directions.

Fig. 3. The HGB4 prototype assembled at the final focal plane of FRS (S4). On the top of the detector under the cover there is the AWAGS electronics.

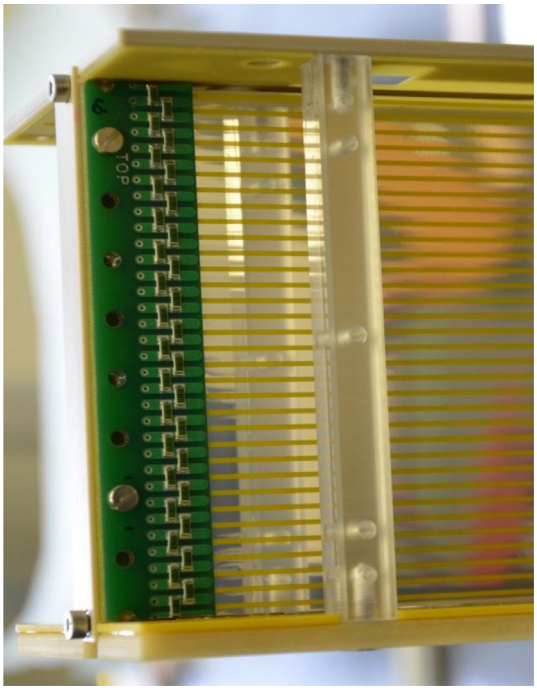

Fig. 4. The field-cage of one GEM-TPC [15].

3. Analysis method

The data from the DUT were recorded as waveforms of each signal. The pedestal and signal amplitude of the waveform were extracted together with the time of arrival at a threshold. The cluster reconstruction was the next step via the execution of the clusterization process. For the clusterization, all the strips belonging to a single event inside the gas volume were grouped and followed by a fitting of a Gaussian function to determine the cluster amplitude profile and its position. This was followed by the track reconstruction, which is needed to compute the extrapolated position at the DUT.

Then the last step was to obtain the spatial resolution, and the detection and tracking efficiencies. The sections below describe in detail all the steps of the methodology used throughout this study.

3.1. Signal flow

The waveform with 1000 samples is shown in Fig. 7(a), i.e. ADC counts as a function of the sampling time. The region of interest of the waveform includes the baseline and the signal samples (~784 samples of the full waveform) for one readout channel. The corresponding distribution in ADC counts of the baseline and signal samples for a single strip is shown in Fig. 7(b). For this distribution, a binning of one bin corresponding to one ADC channel was used. From the samples of the baseline, the pedestal distribution was obtained, and a mean value of 7771.0(3) ADC counts and sigma of 6.9(3) were extracted by using a Gaussian fit as shown in Fig. 7(c). The same method was applied in order to extract the minimum level of the waveform. For example, a mean value of 2689.0(5) ADC counts and sigma of 6.1(5) were obtained (see Fig. 7(d)). The difference between the pedestal and the minimum level of the waveform represent the signal amplitude in the strip.

For a complementary check of the method mentioned above, the waveform was fitted by a sigmoid curve (see Fig. 8, in red dashed line) to determine the amplitude in the strip and compared with the value previously obtained. The waveform was fitted using the sigmoid function

$$f(t) = P_0 + \frac{P_1}{(1 + exp(-\frac{t-P_2}{P_3}))}, \quad (1)$$

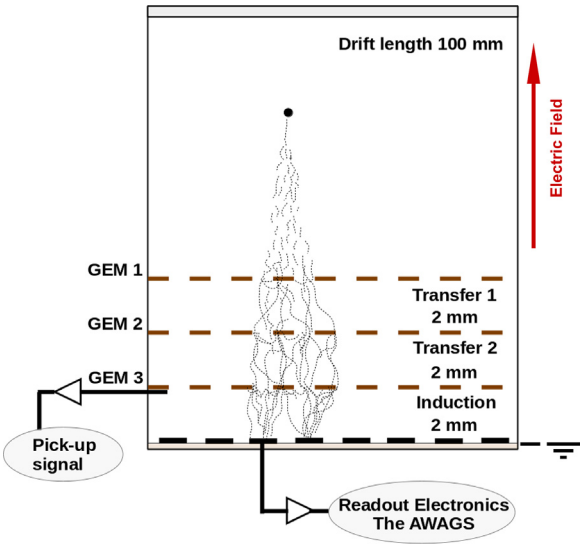

Fig. 5. The layout of the GEM-TPC in the single field-cage configuration. The field-cage, triple GEM stack, and locations for picking up signals are shown.

where $f(t)$ is the fitted curve as a function of time (time bin) t, P_0 is the minimum level of the waveform, P_1 is a value of the signal amplitude, P_2 is the time bin when the maximum slope occurs, and P_3 is the maximum slope parameter.

In Fig. 8 the determined value for the minimum level of the waveform is 2689(6) ADC counts, and the amplitude of the signal is 5080(15) ADC counts. The extracted amplitude is in good agreement with the first mentioned method, which gives the amplitude of 5082.0(6) ADC counts.

Since the values of the pedestals were not constant within a single strip, the sigmas of pedestal distributions were saved for later channel equalization. In conclusion, both methods were found to produce very close results for the signal amplitude, resulting similarly reconstructed clusters as expected.

3.2. Signal timing

Since the sampling rate of the FEBEX3b affects the precision in reconstructing the position in the y direction, two methods to determine the timing of the event were compared. The timing of a single cluster was determined by applying the leading edge method in order to extract the Signal Arrival Time (SAT). The channel used was the closest to the mean value of the reconstructed cluster amplitude distribution. Two SATs were extracted by keeping the threshold at a fixed value of 100 ADC counts. The value of the threshold was selected based on baseline fluctuations.

Time projections of the waveform and fitted sigmoid at the crossing point of the threshold were determined, as shown in Fig. 9. A good comparison between determined times of 1298(20) ns and 1289(15) ns from the waveform and the sigmoid fit crossing points was extracted.

In all three beam positions, the SAT as a function of the cluster amplitude was calculated to check the possible time-walk correction. The lack of slew in the Signal Arrival Time indicates there is no possible time-walk correction to be applied (see Fig. 10).

As a conclusion, for the following analysis, the time of the cluster is determined from the waveform crossing point without the sigmoid fit.

3.3. Clusterization process

The clusterization process is one of the most important steps of the GEM-TPC data analysis. Clusters contain most of the information related to the primary interaction of the beam in the gas volume.

Table 1
Cluster multiplicity fractions and cluster strip multiplicity at different beam positions of the x direction.

Beam position [mm]	Cluster multiplicity [%]			Cluster strip multiplicity [strips]
	1	2	3	
−20	95.15	4.79	0.06	9.80(3)
0	95.68	4.21	0.00	9.79(3)
+20	95.85	4.06	0.09	10.46(5)

From the clusters, it is possible to determine the x position of a particle, the total collected charge, the cluster strip multiplicity, and as a result, the quantity of clusters within one trigger. As an example (see Fig. 11), from a single reconstructed cluster, the mean channel number of 95.800(2), and the sigma of 2.387(3), were determined by fitting a Gaussian function to the amplitude distribution.

The equalization of all strips was done by taking into account the pedestal fluctuations, i.e. baseline fluctuations of each strip per trigger within one run. The first step was to collect all the baseline samples in a distribution for each strip, fit the Gaussian function and extract the sigma of the pedestal. Those sigma values are again collected and fitted by another Gaussian function. The mean of the latter distribution is multiplied by a factor of 150 and yields the sigma cut. This value was then subtracted from the signal amplitude of the strip belonging to a single cluster. This process allowed independent equalization of all channels.

Afterwards, all the strips within a single trigger were grouped, and the Gaussian function fit was applied to determine the corresponding mean strip of the cluster. As a result, the total cluster charge was extracted, and the mean channel of the distribution corresponds to the position in the x direction. In this case, the conversion of the channel to position was done by multiplying the mean channel number by the pitch, which is taken from the geometrical dimensions of the readout strip plane. The Gaussian expression used for fitting the data is the following.

$$f(\mathrm{x}_{strip}) = \frac{A}{C \cdot \sqrt{2 \cdot \pi}} \cdot e^{-0.5 \cdot \frac{(X_{strip} - B)^2}{C^2}}, \tag{2}$$

where A is the maximum amplitude of the mean channel, X_{strip} is the strip channel number, B is the mean channel value, and C is the sigma of the fit.

3.4. Cluster multiplicity and cluster strip multiplicity

The cluster multiplicity is the number of reconstructed clusters within a single scintillator trigger. In Table 1 the cluster multiplicity for the analyzed positions is shown. The fraction of the events with the cluster multiplicity of 1 is about 95% in all positions, while for the multiplicity of 2 is around 4%. For the cluster multiplicity of 3, less than 1% of the reconstructed events were found. The sum of reconstructed cluster fractions is over 99.8% of the triggered events, thus showing high reconstruction efficiency.

The cluster strip multiplicity is the number of strips fired within a single cluster. It is calculated as the total number of strips with position within 3σ of the Gaussian fit. The cluster strip multiplicity distribution for a beam position $x = 0$ mm is shown in Fig. 12 and all positions with a sigma cut of 150 in Table 1. The cluster strip multiplicity varies between 9–11 strips for the positions studied, which is in agreement with what was obtained from simulations [21] using the Garfield++ [22,23] code. The same results were obtained from the procedure with sigmoid fits for each waveform.

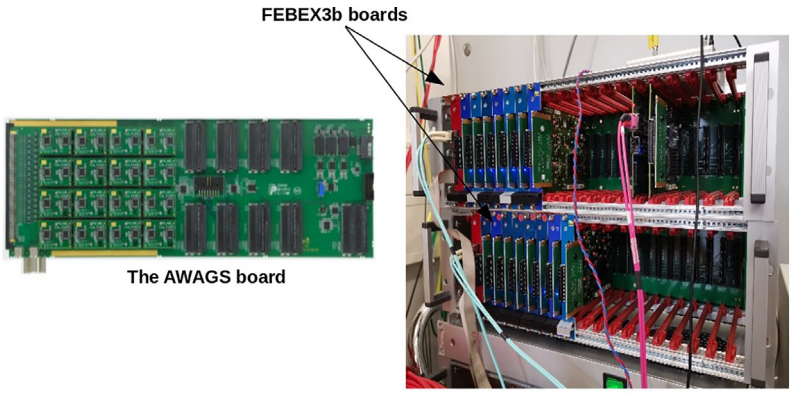

Fig. 6. The AWAGS board is shown on the left and the FEBEX3b boards assembled to the DAQ computer on the right.

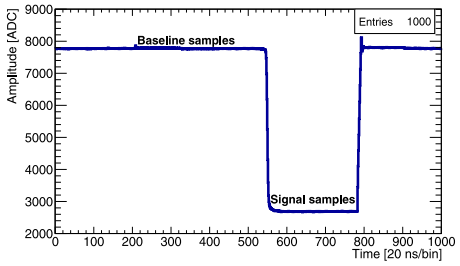

(a) The waveform of an event of a strip, plotted as ADC counts as a function of sampling time.

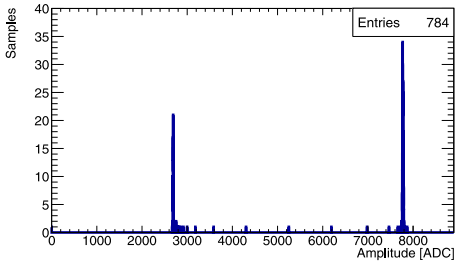

(b) ADC distribution of the baseline and signal of an event in a single strip.

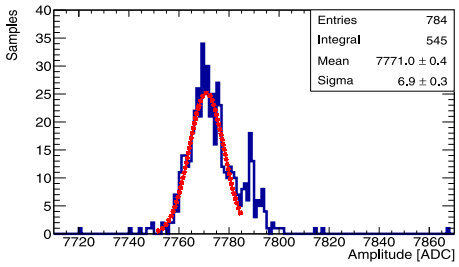

(c) Baseline sample distribution with a Gaussian fit used to determine the mean value of the pedestal.

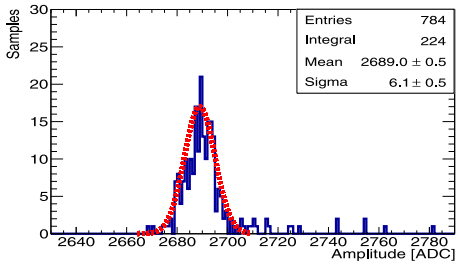

(d) Signal sample distribution with a Gaussian fit used to determine the mean value of the signal.

Fig. 7. Waveform and ADC sample distribution on the top. Baseline sample distribution and signal sample distribution on the bottom.

3.5. Position determination in the TPC and GEM-TPC

The tracking with the conventional TPCs is done by four anode wires, and two readout delay lines [5]. The position in the x direction, i.e. the x coordinate, is determined by the difference between the signal arrival time at both ends of the delay lines. While the determination of the position in the y direction, i.e. the y coordinate, is done by measuring the drift time referenced to the t_0 from the plastic scintillator at the four anode wires, with the latter multiplied by the drift velocity.

The tracking in the GEM-TPC is done by sorting all reconstructed clusters according to their positions. In the x direction, the position assigned to the event is taken from the closest channel to the mean value of the reconstructed cluster as described above (See Fig. 11). The x coordinate is then computed using the following equation

$$X_{GEM-TPC} = B \cdot P_w - D, \tag{3}$$

where $X_{GEM-TPC}$ is the measured x position in GEM-TPC, B is the mean value of the Gaussian fit in the cluster, P_w is the pitch, and D = 51.2 mm is an offset in the x direction defined by the GEM-TPC geometry. Thus, the strip in the middle of the readout strip plane has the x position of 0 mm.

The y coordinate of the DUT is calculated by using the extracted SAT (T_A) as presented earlier (See Fig. 9). The SAT is measured with the strip closest to the mean coordinate channel within the cluster. The y coordinate is then calculated according to

$$f(T_A) = T_A \cdot v_{drift} - y_{offset}, \tag{4}$$

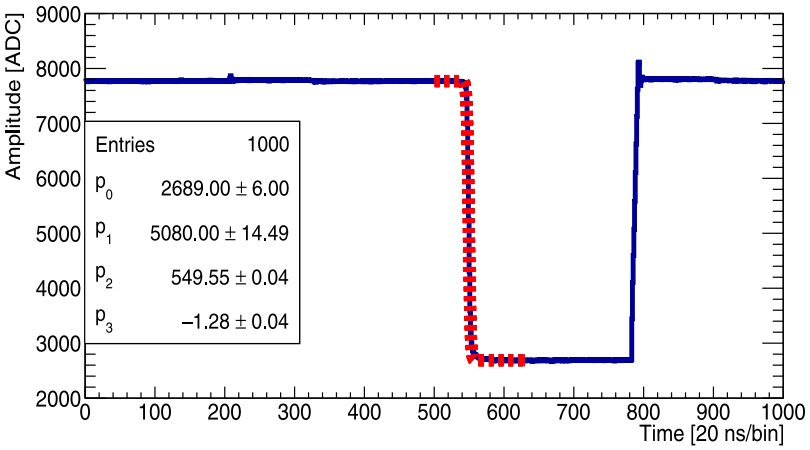

Fig. 8. The waveform of an event with the sigmoid fit.

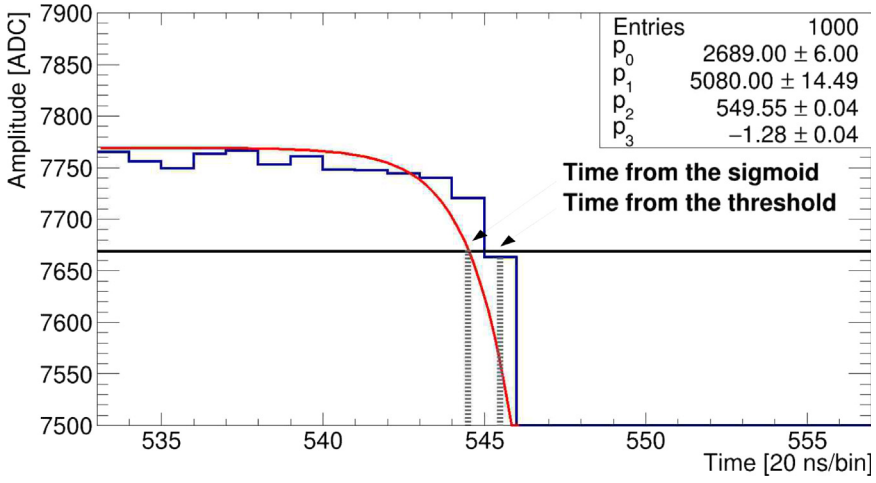

Fig. 9. Signal arrival time determinations with a threshold of 100 ADC counts.

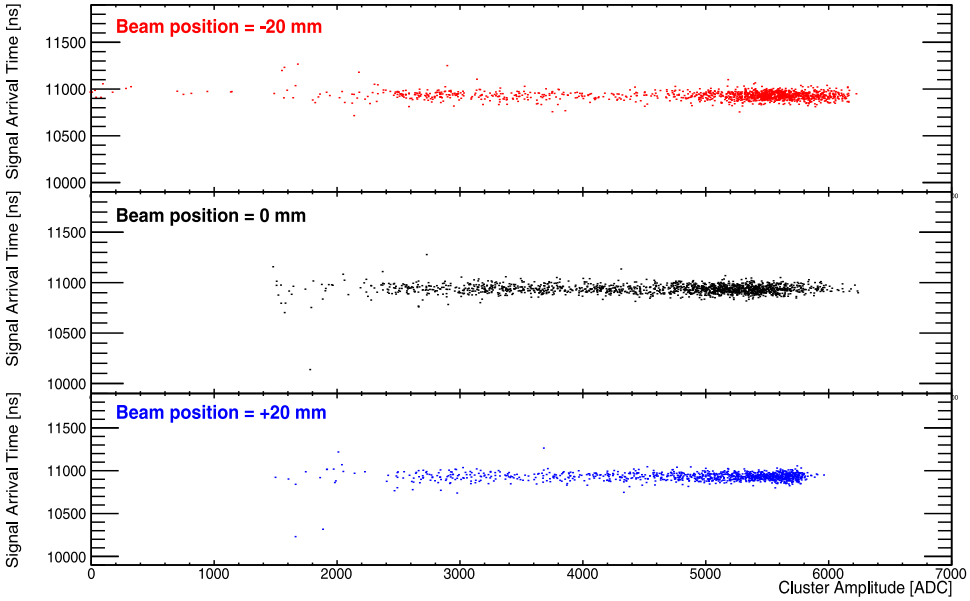

Fig. 10. The signal arrival time distribution as a function of the cluster amplitude at the beam positions −20 mm, 0 mm, and +20 mm of the x direction.

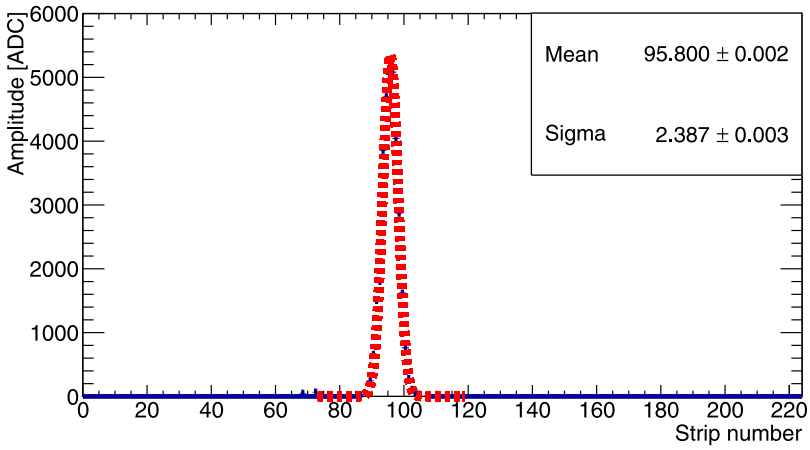

Fig. 11. An example of the reconstructed cluster with a mean channel number of 95.800(2) and sigma of 2.387(3).

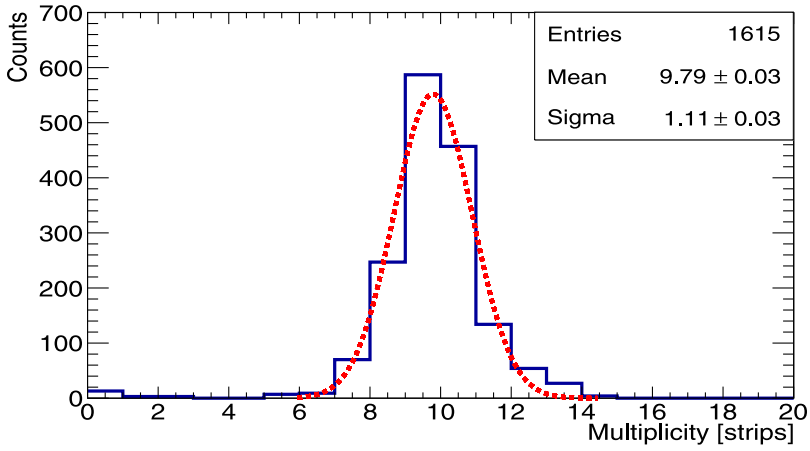

Fig. 12. Cluster strip multiplicity at the beam position of $x = 0$ mm.

where v_{drift} is the extracted drift velocity from data of 5.17(49) $\frac{\text{cm}}{\mu\text{s}}$, and $y_{offset} = 5.01(4)$ cm is the determined offset (see details of the drift velocity extraction in Section 3.6).

3.6. Calibrations of TPCs and GEM-TPC

For the TPCs, the standard calibration method was used [5]. That includes a scintillation fiber grid and a defocused beam, which illuminates the whole area covered by the grid. A calibration grid made of scintillating fibers is placed in the center of the active area of the detector, in front of each TPCs, and the defocused beam is used to illuminate it. The calibration grid has three fibers on the x direction spaced at 12 mm pitch and three on the y direction at 6 mm pitch, each fiber with a 1 mm diameter. Only those particles interacting with the fibers will generate the t_0 triggers and open the acquisition window for recording data.

As a result, three peaks are measured in the x and y directions, corresponding to the positions of scintillating fibers of the calibration grid. From the distributions of events, the mean values of the peaks are extracted using the Gaussian fit to determine the calibration parameters of each delay line and the drift velocity. From the calibration of delay lines, a signal propagation velocity in the delay line is extracted, and a constant offset [5] to convert time into the position in millimeters i.e. to obtain the x coordinate. While for the anode wires, the drift velocity and a constant offset are obtained to convert time into position in millimeters for the y coordinate.

Concerning the TPC42, three peaks were found, with a spacing of 12 mm (see Table 2) with respect to the zero position in the middle as shown in Fig. 13 indicating that the calibration procedure in the x coordinate was successfully carried out.

Table 2
Measured positions of the calibration grid in the x direction at the TPC42 and DUT. The positions of the fibers are determined by a Gaussian fit.

Orientation	Positions at TPC42 [mm]			Positions at DUT [mm]		
	Left	Middle	Right	Left	Middle	Right
X	−12.1(1)	0.0(1)	12.0(1)	−9.7(3)	3.1(3)	15.1(2)

During the calibration of TPC41, it was found that its calibration files measured with the uranium beam were faulty due to unknown reasons. Therefore, it was necessary to take the t_0 trigger from the calibration grid of the TPC42 and project the events on the TPC41. As a result, a similar pattern of the calibration grid is obtained in the TPC41, as shown in Fig. 14.

In the case of the GEM-TPC, the calibration grid of the TPC42 was used by taking the t_0 triggers from the TPC42 and projecting those events into the GEM-TPC. It was found that the difference between the expected drift velocity value of 5.40(1) $\frac{\text{cm}}{\mu\text{s}}$ calculated from the drift field of 122.5 $\frac{\text{V}}{\text{cm}}$ and the measured is of 4(11) %. Hence carrying out the calibration of the drift velocity for the GEM-TPC.

In order to confirm the hypothesis for the preservation of the spacing between fibers, when projecting events from the calibration grid of the TPC42 on the GEM-TPC, the reconstruction of these events were carried out. The measured spacing between fibers in the x direction at the GEM-TPC is shown in Table 2 and in Fig. 15. It can be seen the

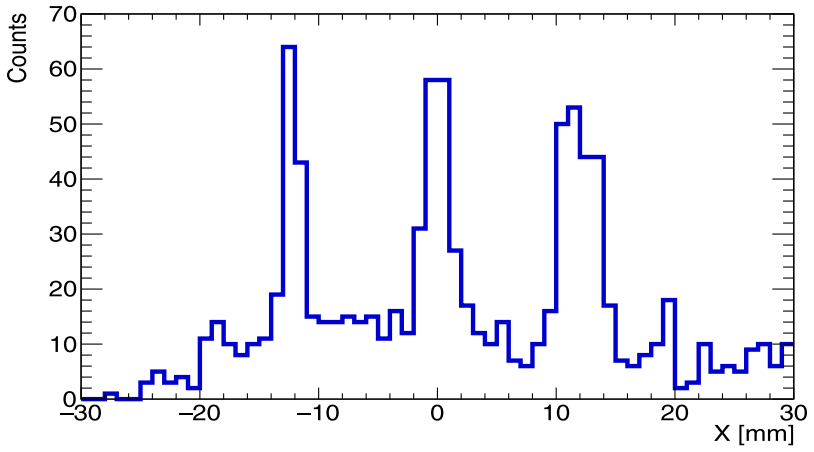

Fig. 13. Calibrated x position spectrum of the TPC42.

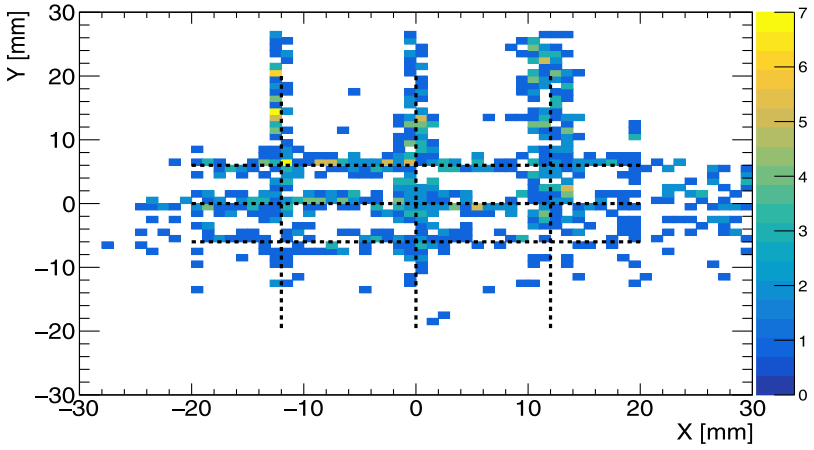

Fig. 14. Calibrated grid positions of the TPC42. From the calibration grid, three wires in the x and y directions are shown with the dashed lines.

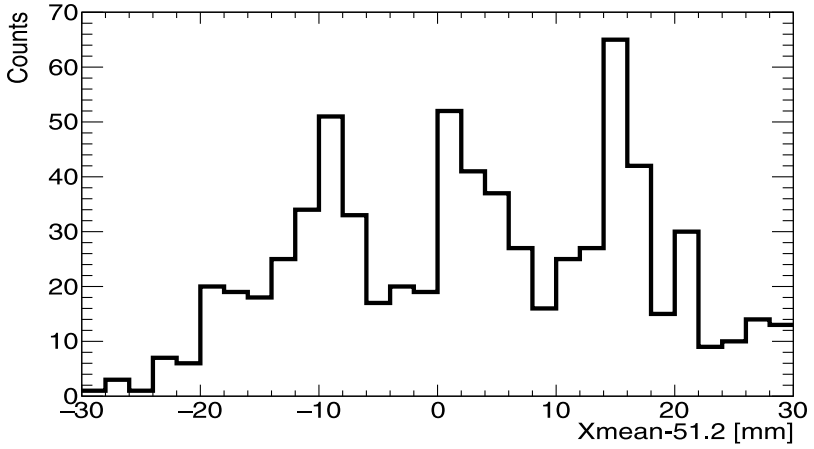

Fig. 15. Measured x position spectrum of the single GEM-TPC when the trigger is taken from the TPC42 calibration grid.

distance between fibers of about 12 mm. Although the defocused beam was used and events are projected, the angle of these events are not well known, and the uncertainty of this projection will increase when the projection distance increases. However, this effect was not pronounced when reconstructing the calibration grid at the GEM-TPC.

In conclusion, in this in-beam test study was found for the first time that with a single calibration grid, it is possible to perform calibration all the detectors of this setup.

3.7. Alignments

Using the measured data at the beam position at $x = 0$ mm, the detectors were realigned in the beam coordinate system starting from the TPCs, which are used as the reference trackers. The goal was to find offsets for the TPCs using the mean value of the residual distribution [24]. The residual is the difference between the measured position at the DUT and the extrapolated position of the event at the

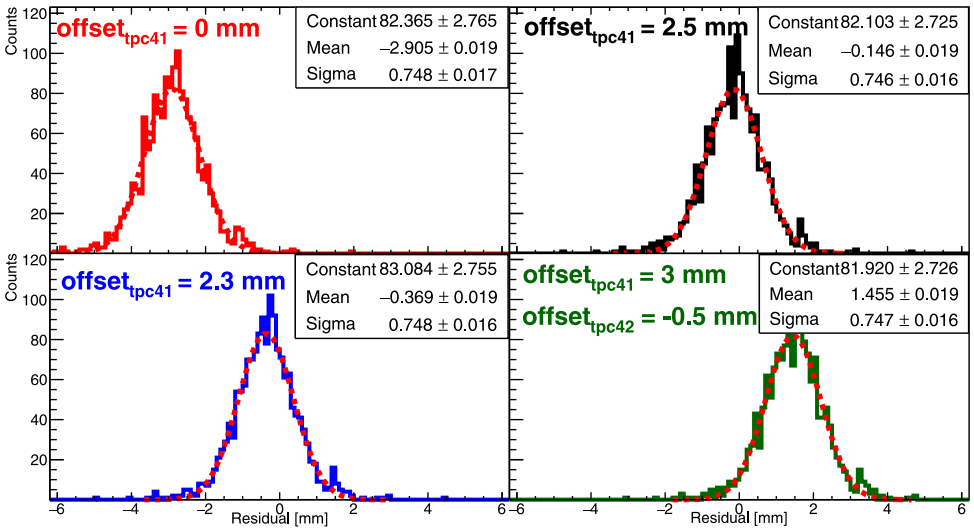

Fig. 16. Residual distributions with the Gaussian fit at the location of the DUT in the x direction during the alignment process. The red distribution shows the measured residual distribution before the offline alignments, and the black one shows the residual distribution with the selected offset of 2.5 mm. The distributions on the bottom are examples of residual distributions during the iterative process.

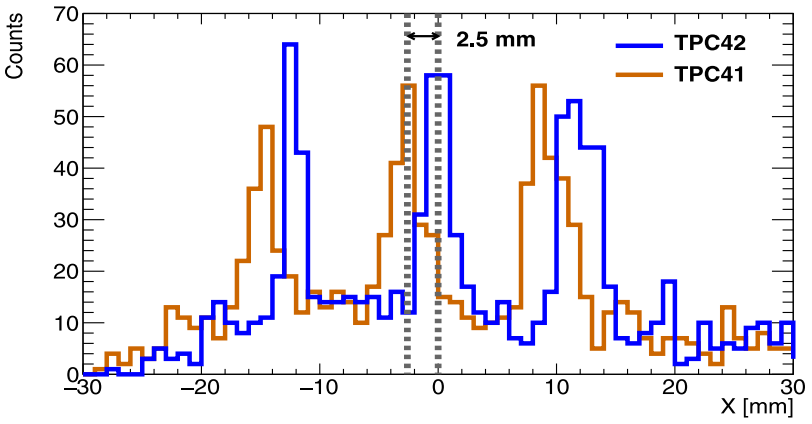

Fig. 17. Measured x positions at the TPCs after the calibrations and alignments when the trigger is taken from the TPC42 calibration grid.

location of the DUT. The procedure used corrects for possible shifts of the TPCs in the x direction. A series of iterative processes were carried out to complete the offline alignment as follows

1. Calculate the extrapolated position using the TPCs for the events at the position of the DUT.
2. Extract the measured position of the events in the DUT.
3. Fill the residual distribution, which is the difference between the extrapolated and measured event positions.
4. If the mean of the residual distribution differs from zero, add the offsets to the TPC positions and continue the iterative process from point 1, until the mean value of residual distribution will become zero.

Fig. 16 shows examples of residual distributions with different offset values at the TPC41 and TPC42 during the offline alignment process. It can be seen that the center of the distributions varies around zero with minor variations of sigma. Additionally, the measured angle with TPCs in the xz plane along the iterative process varied from 4.8 mrad to 1.9 mrad.

As a result of the iterative process, the distances between measured beam positions in the TPCs were calculated in three different locations. Fig. 17 shows the measured positions at the TPCs, after the alignments when the t_0 trigger is taken from the TPC42 calibration grid, and in Fig. 18 at three different positions in the x direction.

The relative offset between the measured beam positions at the TPCs varied by 2.2–4.5 mm. The offset of 2.5 mm for the TPC41 was found to be the best choice. This can be seen in the correlation plot between the extrapolated and measured beam positions at the DUT in Fig. 19 and residual distribution remaining at zero in Fig. 16 (black curve). Furthermore, the beam is on a 45 degree line and crosses the origin point at $x = 0$ mm (see Fig. 19), which is expected in case of good alignment. Despite the good agreement, it can be seen that there is a small difference between the extrapolated and measured positions at the beam locations -20 mm and +20 mm. This discrepancy is caused by the propagation error of different sources, such as the position calibration precision and the error on the extrapolated and measured positions. In conclusion, the cumulative error contribution is relatively small.

4. Spatial resolution and efficiencies

In Fig. 20 the beam profiles of the Uranium projectiles at the position $x = 0$ mm are shown. For this in-beam test, the focal point of the FRS beam was set behind the GEM-TPC in the downstream direction, which can be seen by decreasing the beam spot. To further

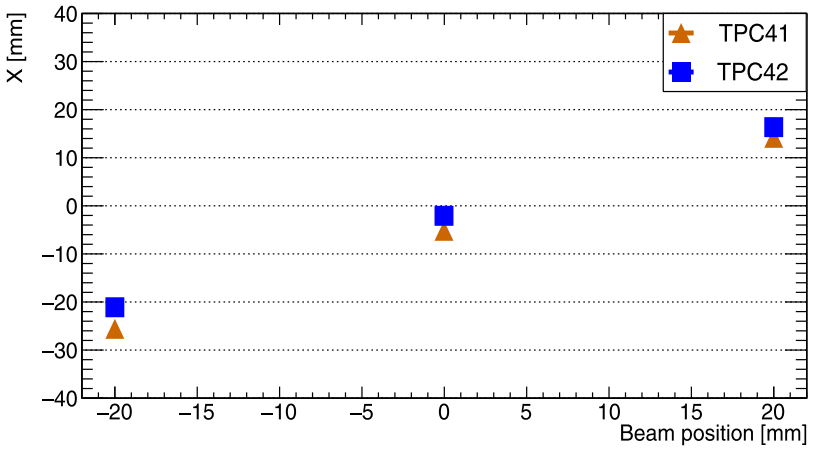

Fig. 18. Measured positions in the x direction at reference TPCs at beam positions of −20 mm, 0 mm, and +20 mm.

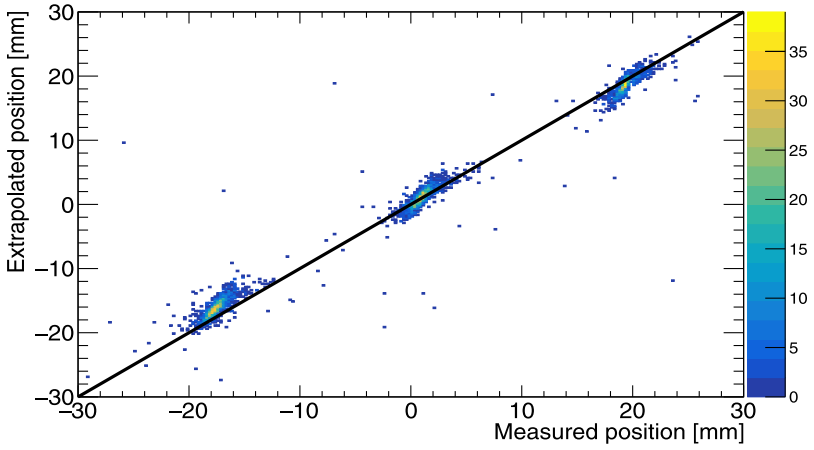

Fig. 19. Correlation plot of the extrapolated and measured beam positions at −20 mm, 0 mm, and +20 mm in the GEM-TPC.

investigate the performance across the whole sensitive area, the beam was moved in different directions on both axes. In the x direction, the beam was moved to positions −20 mm, and +20 mm, in addition to 0 mm used as a reference point. In the y direction the beam was moved to positions −4 mm, +6.5 mm, and +15 mm.

One of the conditions set for the beam profiles was that the cluster multiplicity was equal to one, and for each anode signal of the conventional TPCs, a preselection criterion is applied to their control sum (CS) [5], hence the hits within $3\sigma_{CS}$ were accepted.

4.1. Resolution of the GEM-TPC

The resolution of the GEM-TPC was measured using the conventional TPCs as reference trackers. The resolution can be determined from the standard deviation of the residual distribution, which is the difference between the extrapolated and measured event positions at the location of at the DUT. The extrapolation of the track X_{ext} is done by a linear extrapolation with the equation

$$X_{ext} = \frac{X_{42} - X_{41}}{D_1} \cdot D_2 + X_{42}, \tag{5}$$

where X_{42} and X_{41} are the measured positions in the x direction at the TPCs, $D_1 = 1120$ mm, which is the distance between TPC41 and TPC42, and $D_2 = 1235$ mm, the distance between TPC42 and GEM-TPC along the beam line.

In Fig. 21 is shown the residual distribution at the beam position of $x = 0$ mm, with the $\sigma_{res} = 0.75(2)$ mm. The mean value of the residual distribution shows a small offset still present at $x = -0.15(2)$ mm. The width of the residual distribution σ_{res} contains the quadratic sum of the spatial resolution of the DUT, σ_{dut}, and tracking uncertainty [25] σ_{tr} as following

$$\sigma_{res} = \sqrt{\sigma_{dut}^2 + \sigma_{tr}^2}. \tag{6}$$

Conservative assumption of the tracking uncertainty that it contains only the internal spatial resolutions of TPCs was made. This assumption underestimates the uncertainty of the tracking system, thus decreasing the spatial resolution of the DUT. For the tracking uncertainty determination, the internal spatial resolutions of TPCs were calculated with the method explained in Ref. [5]. The calculated internal spatial resolutions of TPCs at the beam position 0 mm are 81(2) μm for the TPC42 and 75(2) μm for TPC41. Using Eq. (6), the resulting spatial resolution of the DUT is of 0.74(2) mm.

The measured spatial resolution of the DUT in three different positions is shown in Fig. 22. It can be seen that it varies between 0.74–0.81 mm. Moreover, these values remain relatively constant at all three positions. Despite a small disagreement observed in the correlation plot at the positions of −20 mm and +20 mm (see Fig. 19), no strong effects on the measured resolution were found. Additionally, for

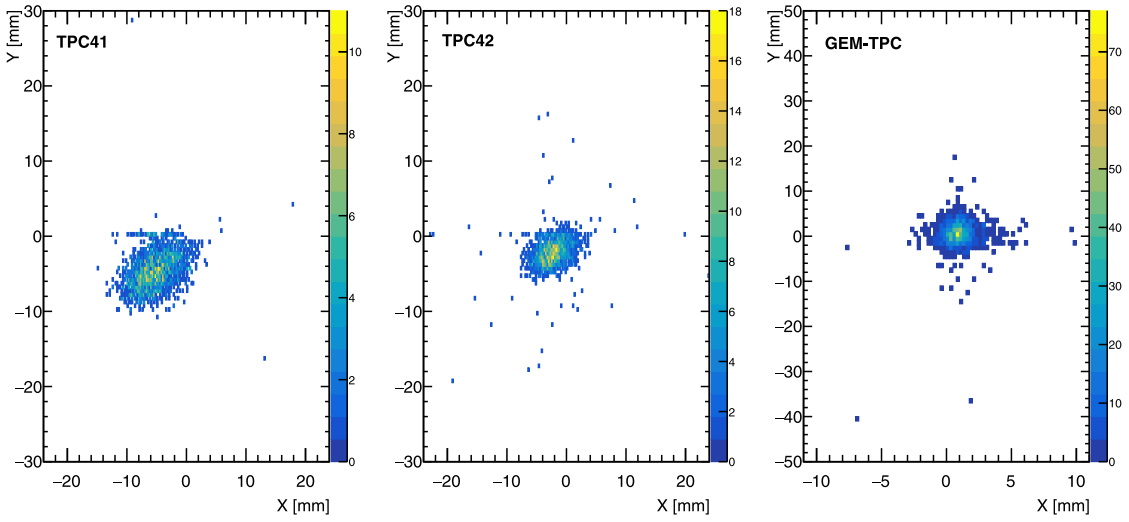

Fig. 20. Beam profiles in the TPCs and GEM-TPC at the beam position $x = 0$ mm.

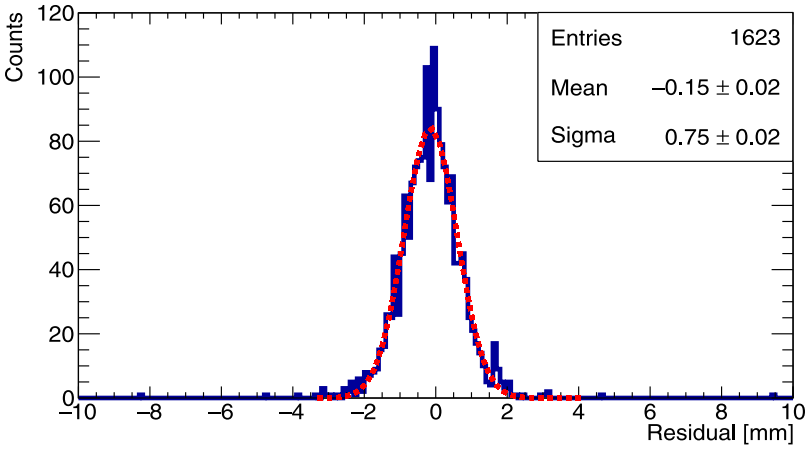

Fig. 21. Residual distribution at the beam position $x = 0$ mm. The determined spatial resolution of the DUT in this position is 0.74(2) mm.

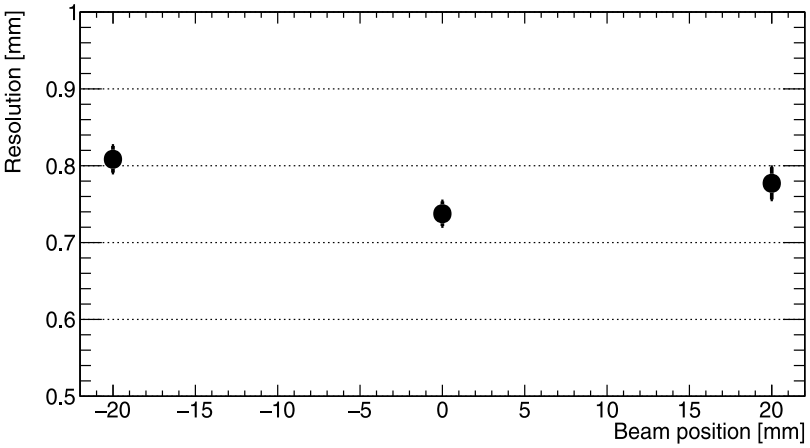

Fig. 22. Measured spatial resolution of the DUT in beam positions -20 mm, 0 mm, and +20 mm, which varies from 0.74(2) mm to 0.81(3) mm.

Table 3
Percentages of the events at the TPC41 and TPC42 simultaneously fulfilling $3\sigma_{CS}$ requirement in all four or only in a subset of the anodes. The sum of the percentages represents the total detection efficiency.

Pos. [mm]	TPC41					TPC42				
	1 Anode	2 Anodes	3 Anodes	4 Anodes	Sum [%]	1 Anode	2 Anodes	3 Anodes	4 Anodes	Sum [%]
−20	0	0.3	0.8	94.9	96.0	0.5	1.1	2.6	93.5	97.7
0	0.1	0.1	0.6	95.2	96.0	0.3	0.8	3.0	89.8	93.9
20	0.6	0.3	1.9	94.5	97.3	0.5	0.9	1.9	91.6	94.9

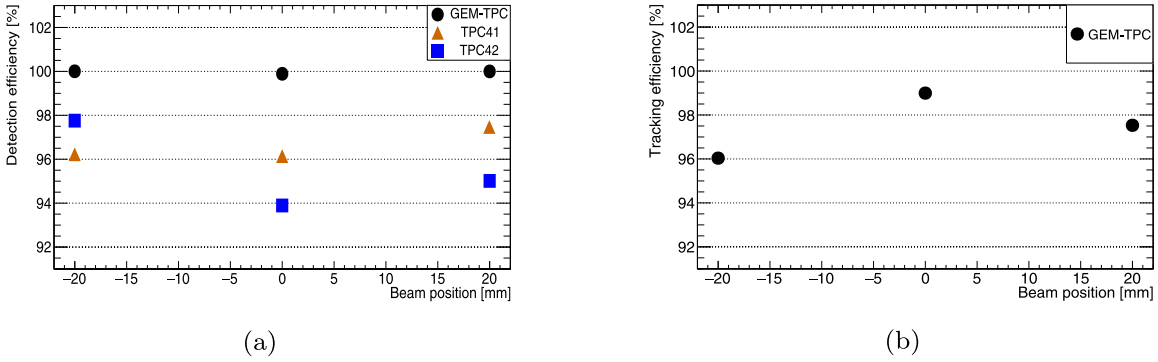

(a) (b)

Fig. 23. The detection efficiencies of the GEM-TPC in the single field-cage configuration and the reference TPCs for three different beam positions are shown on the left. For the GEM-TPC, the detection efficiency is higher than 99.8%. On the right, the tracking efficiency of the GEM-TPC is shown, which varies from 96.0% to 99.0%.

the case with the sigmoid fits, the measured spatial resolution varied from 0.73(2) mm to 0.82(3) mm. Indicating that the difference between the two different analysis methods is very small and as expected.

However, the present results deviate remarkably from earlier measurements obtained from the GEM-TPC prototype HB3, equipped with different readout electronics [11]. The spatial resolution obtained varied between 120 - 300 μm [11] in the x direction. One of the differences between these measurements was that the external spatial resolution of the reference trackers was used for the latter. Another difference was the configuration of the experimental setup, with the GEM-TPC located between the reference trackers.

In conclusion, in the present analysis, it was not possible to perform the standard calibration of the TPC41 with the uranium beam data, thus possibly underestimating its contribution in the extraction of the final resolution value from the sigma of the residual distribution. Moreover, the extrapolation distance for the track reconstructed by the reference trackers TPC41 and TPC42 will significantly affect the precision of the extrapolated position at the DUT [26].

4.2. Detection and tracking efficiency

The detection efficiency of the GEM-TPC is calculated from the ratio of the events at the DUT and triggered events at the scintillator. In contrast, the tracking efficiency is the ratio between the reconstructed cluster position at the DUT associated with the extrapolated track by the TPCs. Moreover, the measured cluster position at the GEM-TPC is required to be within 5σ of the extrapolated track position, where the sigma is the width of the residual distribution.

The tracking efficiency is an important parameter since at the Super-FRS > 95% tracking efficiency at the 1 MHz counting rate is a requirement. The efficiencies are measured at three different beam positions of x = -20 mm, 0 mm, and +20 mm.

In Table 3 the percentages of the events at the TPCs that simultaneously fulfilled $3\sigma_{CS}$ requirement in all anodes or only in a subset of the anodes are shown. Finally, the total sum of the individual percentages represents the detection efficiency for each TPC. It can be seen that the detection efficiency for the TPC41 varies from 96.0% to 97.3%, and for the TPC42 from 93.9% to 97.7%.

Table 1 shows the percentages of cluster multiplicities at the GEM-TPC for each beam position. In total, the quantity of reconstructed clusters was 99.8%–100% of all triggered events, which in this case represents the detection efficiency. The detection efficiencies of the GEM-TPC and the TPCs are shown in Fig. 23(a), whereas the tracking efficiency of the GEM-TPC is shown in Fig. 23(b).

In summary, the GEM-TPC in the single field-cage configuration has the tracking efficiency > 96%, and the detection efficiency > 99.8% in all beam positions.

5. Conclusions

The presented results show that the newly developed clusterization algorithm for this detector performed very well, with over 99.8% of the clusters reconstructed. This method allowed to determine the signal amplitude from the strips in every event. A concurrent method was used to extract the amplitude of the signal using a sigmoid fit yielding similar results. The detection efficiency of 99.8% for the GEM-TPC was achieved on an event-by-event basis, giving confidence for its future use.

As a result, the newly developed electronics can be used in a gaseous detector. However, at a low counting rate due to limitations on the data throughput. This latter can be estimated by the length of each waveform collected for each strip. Furthermore, the plan is to explore all the features of the readout electronics in the newer version of the AWAGS electronics at different in-beam tests with a different digitizer that can match the timing requirements of the GEM-TPC in the future.

We discovered that by using a single calibration grid is possible to calibrate all the detectors in the same setup, which might have either a missing or malfunctioning calibration grid.

The Gaussian fit method was used to determine the position of the reconstructed cluster in the x direction by extracting the mean channel value multiplied by the pitch of the strip.

It was demonstrated for the first time that the position reconstruction in the y direction could be performed using the calibration grid of the closest located reference tracker. Thus, it allowed for determining the drift velocity.

The leading-edge method used to determine the signal arrival time of the cluster was used to reconstruct the event position in the y direction. However, this parameter will be extensively studied in the future.

After determining the positions in the x and y axes of each event, it was possible to reconstruct the beam profile.

The tracking reconstruction at the GEM-TPC yielded the spatial resolution between 0.74(2) mm to 0.81(3) mm, fulfilling one of the requirements for operation at the Super-FRS.

Last but not least, the tracking efficiency exhibited by the GEM-TPC in the single field-cage configuration was over 96%, for all three beam positions, giving confidence for its use. This GEM-TPC will be tested at an increased particle rate in order to find the maximum rate capability in the future.

Declaration of competing interest

The authors declare that they have no known competing financial interests or personal relationships that could have appeared to influence the work reported in this paper.

Data availability

Data will be made available on request

Acknowledgments

Acknowledgments to the FRS team for the broad support during the campaign. Many thanks to H. Weick for beam tuning and Y. Tanaka, who took care of the TPC settings during the test.

References

[1] G. Rosner, Future Facility: FAIR at GSI, Nucl. Phy. B (Proc. Suppl.) 167 (2007) 77–81, http://dx.doi.org/10.1016/j.nuclphysbps.2006.12.089.
[2] H. Geissel, et al., The Super-FRS project at GSI, Nucl. Instr. Meth. Phys. Res. B 204 (2003) 71–85, http://dx.doi.org/10.1016/S0168-583X(02)01893-1.
[3] J. Äystö, Experimental program of the Super-FRS Collaboration at FAIR and developments of related instrumentation, Nucl. Instr. Meth. Phys. Res. B 376 (2016) 111–115, http://dx.doi.org/10.1016/j.nimb.2016.02.042.
[4] H. Geissel, et al., The GSI projectile fragment separator (FRS): a versatile magnetic system for relativistic heavy ions, Nucl. Instr. Meth. Phys. Res. B 70 (1992) 286–297, http://dx.doi.org/10.1016/0168-583X(92)95944-M.
[5] R. Janik, et al., Time Projection Chambers with C-pads for heavy ion tracking, Nucl. Instr. Meth. Phys. Res. A 640 (2011) 54–57, http://dx.doi.org/10.1016/j.nima.2011.02.052.
[6] F. García, et al., IEEE Nuclear Science Symposium Conference Record, (ISSN: 1095-7863) 2009, pp. 269–272.
[7] Conceptual Design Report for the Scientific Program of the Super-FRS Experiment Collaboration, GSI Rep. (3) (2016) http://dx.doi.org/10.15120/GSI-2016-03763.
[8] O. Kiselev, et al., Radiation hardness tests of Si detectors for Time of Flight measurements at the Super-FRS, 2014, p. 137, MU-NUSTAR-FRS-03.
[9] M. Pfutzner, et al., Energy deposition by relativistic heavy ions in thin argon absorbers, Nucl. Inst. Meth. Phys. Res. B 86 (3) (1994) 213–218, http://dx.doi.org/10.1016/0168-583X(94)95280-9.
[10] In-beam test of the TwinTPC at FRS, in: GSI scientific report 2014, 2014, p. 500.
[11] F. García, et al., A GEM-TPC in twin configuration for the Super-FRS tracking of heavy ions at FAIR, Nucl. Instr. Meth. Phys. Res. A 884 (2018) 18–24, http://dx.doi.org/10.1016/j.nima.2017.11.088.
[12] P. Wieczorek, H. Flemming, H. Deppe, Low Noise Amplifier with Adaptive Gain Setting - (AWAGS) ASIC, in: TWEPP 2021, 2021.
[13] E. Rocco, et al., AWAGS: A single ASIC to identify fast ions from protons to uranium, Nucl. Instr. Meth. Phys. Res. A 1040 (2022) http://dx.doi.org/10.1016/j.nima.2022.167188.
[14] F. Sauli, GEM: A new concept for electron amplification in gas detectors, Nucl. Instr. Meth. Phys. Res. A 386 (1997) 531–534, http://dx.doi.org/10.1016/S0168-9002(96)01172-2.
[15] F. García, et al., The Super-FRS GEM-TPC prototype development - TDR, 2016, http://dx.doi.org/10.48550/ARXIV.1612.05045.
[16] J. Hoffmann, FEBEX3b, specification. https://www.gsi.de/fileadmin/EE/Module/FEBEX/febex3b.pdf. (Accessed on September 1st, 2022).
[17] I. Rusanov, et al., FPGA Hit Finder and Energy Filter for the FEBEX Pipelining ADC, FG-CS-04 GSI scientific report, 2013, http://dx.doi.org/10.15120/GR-2014-1-FG-CS-04.
[18] H.G. Essel, N. Kurz, The general purpose data acquisition system MBS, IEEE Trans. Nucl. Sci. 47 (2) (2000) 336, http://dx.doi.org/10.1109/23.846176.
[19] S. Minami, et al., Design and implementation of a data transfer protocol via optical fiber, in: 2010 17th IEEE-NPSS Real Time Conference, 2010, pp. 1–3, http://dx.doi.org/10.1109/RTC.2010.5750447.
[20] J. Hoffmann, TRIXOR, PC-based Trigger Module. Available at https://www.gsi.de/fileadmin/EE/Module/TRIXOR/trixor.pdf. (Accessed on September 1st, 2022).
[21] A. Prochazka, et al., Simulations of the GEM-TPC response, GSI SCIENTIFIC REPORT 2013, 2014, http://dx.doi.org/10.15120/GR-2014-1-FG-S-FRS-12.
[22] R. Veenhof, Garfield - simulation of gaseous detectors. https://Garfield.Web.Cern.Ch/Garfield/. (Accessed on December 30th, 2022).
[23] Garfield++ software. https://Garfieldpp.Web.Cern.Ch/Garfieldpp/. (Accessed on September 1st, 2022).
[24] R. Farinelli, et al., GRAAL: Gem reconstruction and analysis library, J. Phys. Conf. Ser. (ISSN: 1742-6596) 1525 (1) (2020) 012116, http://dx.doi.org/10.1088/1742-6596/1525/1/012116.
[25] J. Kaminski, et al., Study of various anode pad readout geometries in a GEM-TPC, IEEE Trans. Nucl. Sci. 52 (6) (2005) 2900–2906, http://dx.doi.org/10.1109/TNS.2005.862797.
[26] J.R. Taylor, An Introduction To Error Analysis, second ed., University Science Books, ISBN: 978-0-935702-42-2, 1997.